JOURNAL OF COMPUTATIONAL PHYSICS 122, 83–95 (1995)

Spectral Element Methods for Elliptic Problems in Nonsmooth Domains

D. PATHRIA AND G. E. KARNIADAKIS

Division of Applied Mathematics, Brown University, Providence, Rhode Island 02912

Received July 5, 1994; revised February 9, 1995

Engineering applications frequently require the numerical solution of elliptic boundary value problems in irregularly shaped domains. For smooth problems, spectral element methods have proved very successful, since they can accommodate fairly complicated geometries while retaining a rapid rate of convergence. Geometric singularities, however, often give rise to singular solutions. The accuracy of the spectral element methods is then degraded, and they offer no apparent advantage over low-order finite element methods. In many cases, however, the singular structure of the solution is known, and its form may be exploited by the spectral element method. Among the various ways of doing so (through supplementary basis functions, eigenfunction expansions, and graded meshes), the method of auxiliary mapping proves to be particularly effective. For certain simple cases, the problem is transformed to a coordinate system in which the solution is analytic, and exponential convergence is recovered. Even when this is not possible, the singularity is usually much weaker after mapping, so that other treatments are more effective in the new coordinate system. In this paper, we study different ways of treating singularities, and in particular, the method of auxiliary mapping coupled with the use of supplementary basis functions. Error estimates are presented explaining why the combined approach is more effective, and these estimates are confirmed through a number of numerical experiments for the Laplace, Poisson, and Helmholtz equations.

1. INTRODUCTION

Traditional numerical methods for solving partial differential equations can be classified as being either local or global in nature. Local methods, such as finite difference and finite element schemes, can adapt to fairly arbitrary geometries, but are generally of low order so that the cost of obtaining highly accurate solutions can be prohibitive. Global methods, on the other hand, are of high order, but suffer from their restriction to simple domains. The spectral element method, a particular implementation of the p-version of the h-p method, was proposed to circumvent this restriction. It can accommodate reasonably complicated domains while exhibiting a convergence rate, with respect to polynomial degree, that is faster than an algebraic method for smooth solutions [20].

Shock waves in compressible flow problems, giving rise to the celebrated Gibbs phenomenon, are perhaps the most notorious source of trouble for spectral and spectral element methods. (Although some progress in the construction of high-order nonoscillatory schemes has been made [4, 23], the problem is far from resolved). Singularities are also evident in many incompressible flows; a striking example is flow over an array of *shark-fin shaped riblets in drag-reduction experiments* (Fig. 1). As the width of the riblet tip becomes infinitesimal, the shear stress grows without bound locally, but this results in an $O(1)$ error *globally*. These errors are readily traced to the irregularity of the domain and are manifestations of the basic problems of using polynomial approximations for nonsmooth functions.

We shall concentrate therefore on elliptic problems, interesting in their own right, and also the main source of computational effort when the incompressible Navier–Stokes equations are solved by operator splitting [13]. For such problems, irregularities may be due to the presence of nonsmooth coefficients or nonsmooth forcings, or to abrupt changes in the boundary conditions or boundary shape; whatever their source, the performance of the spectral element method rapidly deteriorates. We shall consider here those singularities that are due to singularities in the geometry; all other data in the problem is assumed to be smooth. In particular, we are interested in corner singularities; typically, first derivatives are unbounded when the angle is reflexive and second derivatives, when the angle is acute or obtuse.

By using a multidomain implementation, we do not incur any real loss of generality or applicability if we focus on a geometry containing just one singular corner. We shall take our domain Ω to be an open, simply connected region in $\mathbb{R}^2$, with the corner situated at the origin and with one arm lying along the positive x-axis, the other at an angle $\alpha\pi$, $0 < \alpha < 2$, in the counterclockwise direction to the first. The boundary may be decomposed as $\Gamma = \overline{\Gamma_1 \cup \Gamma_2}$, where Γ_1 comprises the two edges adjoining the vertex and $\Gamma_2 = \partial\Omega \backslash \Gamma_1$ (see Fig. 2).

In this setting, it is natural to work in polar coordinates (r, θ), since in the vicinity of the corner, the solution typically has the asymptotic form

$$u(r, \theta) \sim c_1 r^{\beta} \zeta(\theta) \chi(r, \theta), \tag{1}$$

where c_1 is some constant, $\zeta(\theta)$ is a smooth function, and $\chi(r,$

0021-9991/95 $12.00

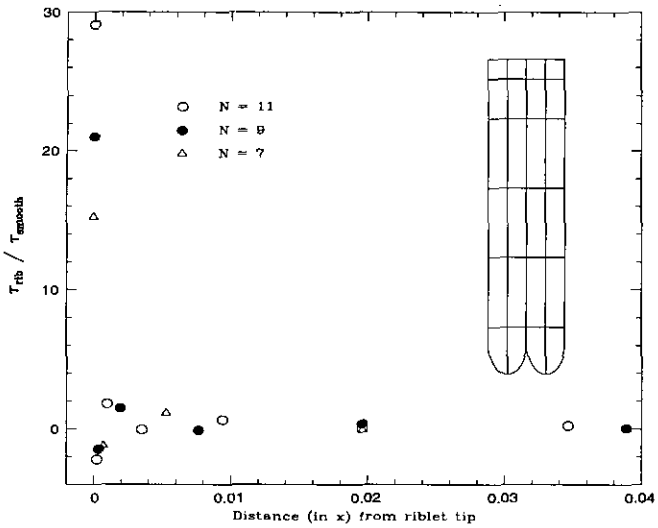

FIG. 1. Oscillations in the shear stress distribution in flow over an array of shark-fin riblets. The inset shows a portion of the domain, which is extended periodically in the horizontal direction. The elemental decomposition is marked in the inset, and N indicates the polynomial degree used within each element.

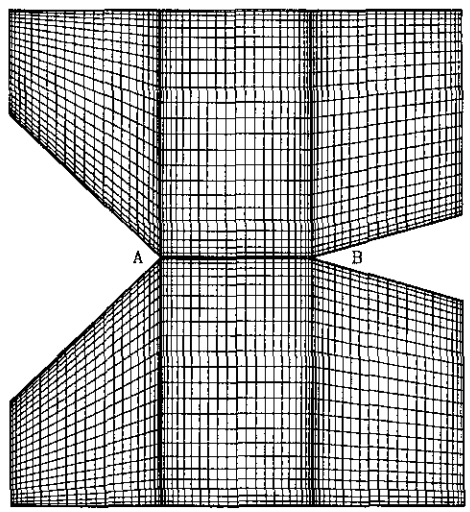

FIG. 3. An example of a spectral element discretization, on a domain containing two re-entrant corners A and B, using six elements with $N = 25$.

θ) is a smooth cutoff function. In this case, it is known that, for a fixed elemental decomposition, the spectral element solution $u_N(r, \theta)$, computed with polynomials of degree N in each element, satisfies

$$\|u_N(r, \theta) - u(r, \theta)\|_{\mathcal{H}^1(\Omega)} \leq c_2 N^{-2\beta-\varepsilon}, \tag{2}$$

where c_2 is a positive constant independent of N and ε is any positive number [3]. The estimate (2) is sharper than the usual spectral error estimates [16], and it precisely captures the convergence rates seen in our numerical experiments. Of course, when the solution is analytic, the standard estimate specifies the faster than algebraic rate of error decay.

The power β depends both on the equation and on the angle α; for most problems discussed here, $\beta = 1/\alpha$ and the convergence rate lies between $O(N^{-1})$ and $O(N^{-2})$. It is possible, however, to use *a priori* knowledge of the value of β in constructing schemes that improve on this convergence rate. This has been done in various ways (see [24, 6]), with three main techniques incorporating: the use of supplementary basis functions; conformal maps to smooth the singularity; and various forms of domain subdivision (h-refinement) to compensate for the singularity. We shall discuss these techniques in more detail as they arise in the following sections.

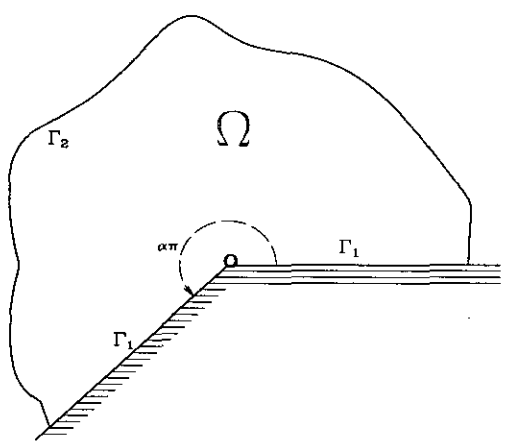

FIG. 2. The model domain Ω consisting of a single corner of angle $\alpha\pi$.

The paper is structured as follows. In Section 2, we outline the key steps in the multidomain spectral element solution of the Helmholtz problem, without any special treatment for the singularity. In Section 3, we review the method of auxiliary mapping, a highly effective technique of improving convergence rates for the corner problem for Laplace's equation. We also mention the limitations of the method used alone, and in Section 4, we discuss the improvements, in the context of the Poisson equation, that come from supplementing the mapping with other techniques. In Section 5, we consider the modifications necessary for the Helmholtz equation, and we close with a few general observations in Section 6, mentioning the extension of the techniques described herein to more general (vector) settings.

2. NUMERICAL PROCEDURE

The numerical solution of the elliptic problem is based on the spectral element method originally proposed by Patera [20], which can be viewed as a particular implementation of the p-version of the h-p finite element method. The method proceeds by first tessellating the domain Ω into four-sided macro-sized *elements* (see Fig. 3), each of which may then be mapped to the unit square by a smooth or isoparametric mapping. Within

each square, the problem is solved using an $N \times N$ spectral approximation, formulated through a tensor-product Lagrangian polynomial representation using the Gauss–Lobatto–Legendre interpolation points. C^0 continuity is enforced strongly at element interfaces, and weak C^1 continuity follows from the problem statement.

Consider the solution of the Helmholtz equation in two dimensions,

$$\nabla^2 u - \lambda u = f, \tag{3}$$

subject to Dirichlet boundary conditions, $u = 0$ on $\partial\Omega$. Let $P_N(\Omega)$ be the space of functions which are (i) tensor products of degree N polynomials in x and y on each standardized element, (ii) C^0 on Ω, and (iii) vanish on $\partial\Omega$. The approximate solution u_N, is the unique member of $P_N(\Omega)$ that satisfies the weak form of the problem

$$\int_\Omega (\nabla u_N \cdot \nabla v + \lambda u_N v + fv)\, d\Omega = 0$$

for all test functions $v \in P_N(\Omega)$. It is known that, if $u \in \mathcal{H}^\sigma(\Omega)$ and if $f \in \mathcal{H}^\gamma(\Omega)$, the numerical solution satisfies

$$\|u - u_N\|_{\mathcal{H}^1(\Omega)} \leq c(N^{1-\sigma}\|u\|_{\mathcal{H}^\sigma(\Omega)} + N^{-\gamma}\|f\|_{\mathcal{H}^\gamma(\Omega)}), \tag{4}$$

where c is some positive constant [16]. Consequently, when the elemental subdivision is fixed, the error decays faster than any power of N for solutions that are analytic in x and y. We shall be primarily interested in this p-response, as opposed to the error as a function of elemental discretization (see [11, 14] for a description of the latter).

A multidomain approach is appropriate in the presence of nonsmooth boundary data since it permits specific treatments to be applied locally; it is practically essential for complicated geometries such as the one shown in Fig. 3. The domains we shall use are disjoint and nonoverlapping, and the solutions are computed independently on each, coupled only through interface conditions. The coupling is based on the iterative relaxation procedure proposed by Funaro, Quarteroni, and Zanolli [9] for elliptic problems, in which a sequence of Dirichlet–Neumann problems is iterated to convergence. Continuity of normal derivatives is enforced at each step, and the iteration proceeds until C^0 continuity is achieved to some prescribed tolerance. The solution procedure can be modified to allow parallel implementation as in [12]. If the Helmholtz problem is solved on two adjacent domains Ω_1 and Ω_2 having common boundary $\Gamma_{1,2}$, the solution, at the m^{th} stage, is made up of a computation step, with the domains treated independently,

$$\begin{aligned} \nabla^2 u_1^m - \lambda u_1^m &= f \quad \text{in } \Omega_1 \\ \nabla^2 u_2^m - \lambda u_2^m &= f \quad \text{in } \Omega_2, \end{aligned} \tag{5}$$

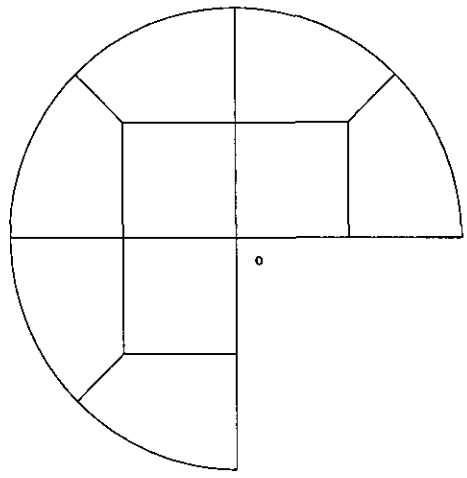

FIG. 4. A domain containing a re-entrant corner at the origin, with $\alpha = \frac{3}{2}$, divided into nine four-sided elements.

followed by a patching step entailing communication between the two processes

$$\left.\begin{aligned} u_1^m &= \delta^m u_2^{m-1} + (1-\delta^m) u_1^{m-1} \\ \frac{\partial u_2^m}{\partial n} &= \frac{\partial u_1^{m-1}}{\partial n} \end{aligned}\right\} \quad \text{on } \Gamma_{1,2}. \tag{6}$$

The relaxation parameter δ^m is chosen dynamically to accelerate the convergence. Specifically, it is the unique real minimizer of the error between successive iterates and is computed as

$$\delta^m = \frac{(e_1^m, e_1^m - e_2^m)}{\|e_1^m - e_2^m\|^2}, \tag{7}$$

where $(\cdot, \cdot)$ denotes the usual L^2 inner product and where e_i^m denotes the difference between successive iterates $e_i^m = u_i^m - u_i^{m-1}$ on the relevant subdomain Ω_i. The computation–communication tasks (5)–(6) are iterated until the solutions on the two domains agree to within some prescribed tolerance along the interface (we used 10^{-12} in our experiments).

For convenience, we have chosen our singular domains to be circular sectors about each singular corner. Such a domain may be broken into quadrilateral elements by the discretization in Fig. 4, which still maintains spectral convergence rates. The Neumann conditions in the patching procedure were imposed in the corner domains and Dirichlet, on the external (background) domain.

3. THE METHOD OF AUXILIARY MAPPING

Laplace's equation

$$\nabla^2 u = 0 \tag{8}$$

in two dimensions serves as the primary test for methods designed to reduce singular effects. The problem has been dealt with successfully by various techniques, all of which make use of the well-known asymptotic behavior of u as $r \to 0$ [2, 19]. The general solution of (8) in the neighborhood of a corner can be expressed as

$$u(r, \theta) = \sum_{k=0}^{\infty} a_k \psi_k(r, \theta),$$

where the coefficients a_k are determined by the (global) boundary conditions and where the fundamental solutions $\psi_k(r, \theta)$ are given by

$$\psi_k(r, \theta) = \begin{cases} r^{k/\alpha} \sin\left(\frac{k}{\alpha}\theta\right) & \text{if } \frac{k}{\alpha} \notin \mathbf{Z} \\ r^{k/\alpha}\left(\ln r \sin\left(\frac{k}{\alpha}\theta\right) + \theta \cos\left(\frac{k}{\alpha}\theta\right)\right) & \text{if } \frac{k}{\alpha} \in \mathbf{Z} \end{cases} \quad (9)$$

for $k = 1, 2, \ldots$ [10]. The solutions in this sequence are increasing in regularity, with $\psi_k(r, \theta) \in \mathcal{H}^{k/\alpha+1-\varepsilon}(\Omega)$ for any real $\varepsilon > 0$. Moreover, as the intruding angle becomes sharper, the regularity of each basis function generally decreases and, as a result, so does the overall convergence rate.

We shall, unless stated otherwise, assume Neumann or Dirichlet boundary conditions along Γ_2, defined such that no singularity is introduced away from the corner. We shall also assume that the solution vanishes along the wedge walls,

$$u|_{\Gamma_1} = 0. \quad (10)$$

This no-slip boundary condition implies that the functions in (9) involving logarithmic terms do not contribute to the solution, and

$$u(r, \theta) = \sum_{k=1}^{\infty} a_k r^{k/\alpha} \sin\left(\frac{k}{\alpha}\theta\right). \quad (11)$$

The crucial observation now is that the simple mapping $z = \xi^\alpha$, which is conformal at all points save the origin, renders the fundamental solutions analytic in terms of the new variables. Under this map, the original domain of Fig. 1 in the $z = re^{i\theta}$ plane is transformed to a semicircle in the $\xi = \rho e^{i\phi}$ plane (see Fig. 5) and the solution in terms of the new variables,

$$u(\rho, \phi) = \sum_{k=0}^{\infty} a_k \rho^k \sin(k\phi),$$

can be numerically approximated without the effects due to the corner singularity.

The auxiliary mapping technique, used as early as 1965 for solving the eigenvalue problem $\nabla^2 u - \lambda u = 0$ [21], was first applied to finite difference solutions of the Laplace and Poisson equations in 1967 [17]. In these early experiments, however, the mapping was applied globally, so that the original domain typically transformed into a peculiarly shaped geometry and, more importantly, the technique was limited to problems with only one singular corner. A multidomain implementation, with isolated treatment of each corner, was developed for the p-version of the h-p method by Babuska and Oh, using wedge-shaped elements [2], and extended by Cai, Lee, and Oh to couple finite element solutions on singular domains with spectral solutions computed on rectangular domains free of singularities [5]. Here we use spectral element simulations in all domains, with the appropriate conformal mapping applied in those which contain a singular corner. The changes to the usual spectral element code are modest. The elemental discretization is normally specified through four corner points; these and the curvature information are mapped straight away to ξ space, where a regular discretization and solution is then performed. The normal derivatives are returned to physical coordinates for the Zanolli patching procedure, and the grid is mapped back to physical space for output purposes.

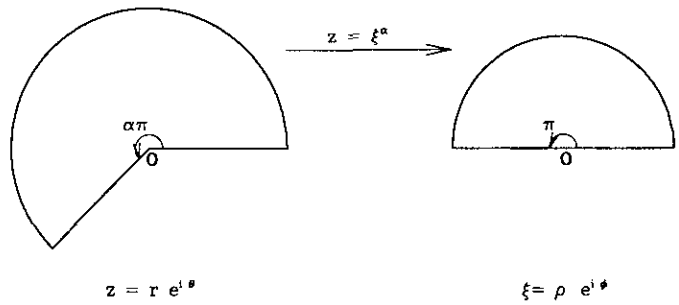

FIG. 5. Mapping of the subdomain containing a singular corner to one in which the corner and its effects have been removed.

EXAMPLE 3.1. We begin with an example of Babuska and Oh [2], solving Laplace's equation on an L-shaped domain with boundary conditions as shown in Fig. 6. A two-domain decomposition was used to compute the numerical solution, with the exterior domain Ω_1 comprising the six large elements furthest from the origin and with the interior domain Ω_2, the nine elements closest to it. The mapping treatment is only applied to Ω_2. In this case, the exact solution is not known so we use a high resolution ($N = 27$) numerical solution as our benchmark. Error plots with and without mapping in the exterior domain Ω_1 and in the interior domain Ω_2 are shown in Fig. 7. Without mapping, the leading order term in the solution behaves as $r^{3/2}$, and the theoretically predicted convergence is $O(N^{-4/3-\varepsilon})$. According to a least squares fit for the exponent, we find $\|u - u_N\|_{\mathcal{H}^1} \approx 1.089N^{-1.615}$ in the domain containing the singular corner, and this contaminates the solution in the exterior domain as well. With mapping, the error appears to decay

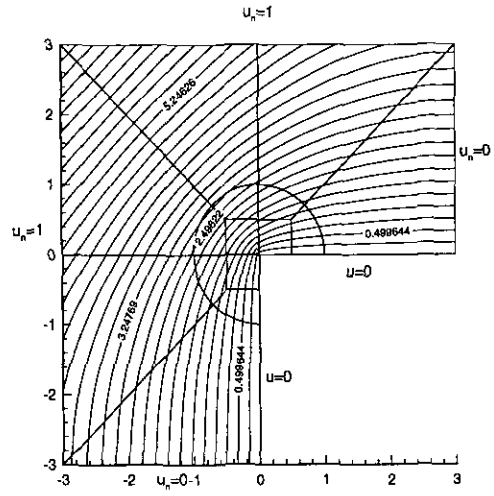

FIG. 6. Domain and boundary conditions for the solution of Laplace's equation.

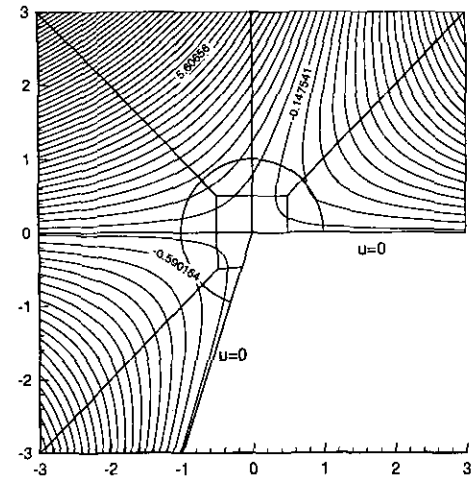

FIG. 8. Domain and numerically computed solution for the problem $\nabla^2 u = 1$, whose exact solution $u = y(y - 3x)/2$ is analytic.

at an exponential rate; a fit of $\|u - u_N\|_{\mathcal{H}^1} \approx 0.426e^{-12.924N}$ is calculated in the interior domain, and a very similar figure is obtained for the external domain as well.

It is easy, however, to cook up problems in which the mapping actually has detrimental effects, for instance, when the solution is smooth in z-space. Components that are smooth in the original coordinates become (weakly) singular through the mapping. What has been neglected up till now is the behavior of the coefficients a_k which are determined by the global boundary conditions. While it is true that the representation (11) converges uniformly to the exact solution as long as Neumann boundary conditions on Γ_2 are in $L^2(\Gamma_2)$, it is not necessarily true that the coefficients decay quickly. Since there is a certain duality between smooth boundary conditions and smooth driving forces (see Appendix A), we shall examine this deterioration in the context of the Poisson equation.

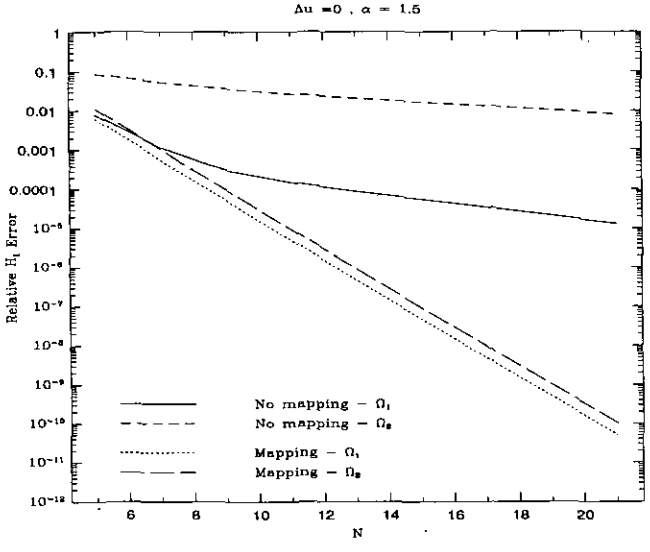

FIG. 7. $\mathcal{H}_1$ errors for the solution of Laplace's equation on the L-shaped domain, with and without auxiliary mapping. In the mapped case, the mapping was applied only to the domain containing the corner.

4. POISSON'S EQUATION

The situation becomes more complicated when a forcing function is introduced as in Poisson's equation,

$$\nabla^2 u = f(x, y). \tag{12}$$

When f is a smooth function, it follows by the shift theorem that u must have some smooth component in addition to the singular structure of the homogeneous solution. The convergence achieved through auxiliary mapping is no better than algebraic, because this regular component becomes irregular upon mapping. In terms of the new coordinates, the equation has a singular forcing function,

$$\nabla^2 u = \alpha^2 \rho^{2\alpha-2} f(x(\rho, \phi), y(\rho, \phi)), \tag{13}$$

and the solution must also exhibit some irregularity. In view of the spectral element convergence estimate (4), it follows that the convergence is algebraic, but this estimate is not optimal and, given the form of singularity, we infer from (2) the improved estimate

$$\|u - n_M\|_{\mathcal{H}^1(\Omega)} \leq cN^{-4\alpha-\varepsilon} \tag{14}$$

for any $\varepsilon > 0$.

EXAMPLE 4.1. Consider what happens if we try to solve $\nabla^2 u = 1$ on the domain shown in Fig. 8, where the re-entrant corner at the origin has $\alpha = 1 + \tan^{-1} 3$. We decompose the

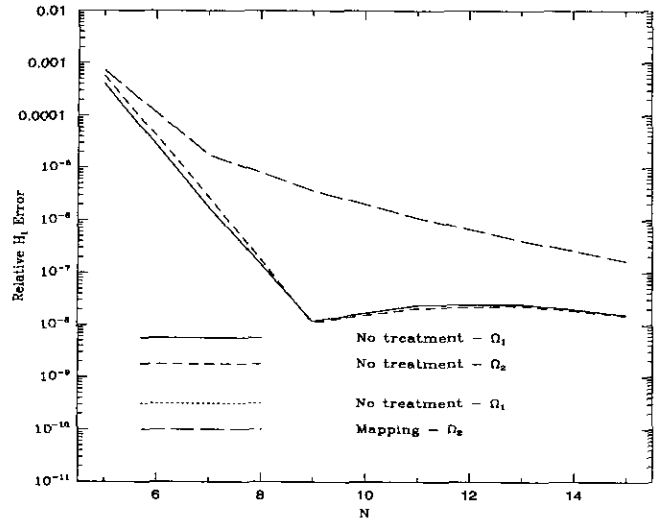

FIG. 9. Relative $\mathcal{H}_1$ errors for $\nabla^2 u = 1$ when $u = y(y - 3x)/2$, for the exterior domain Ω_1 and the interior domain Ω_2.

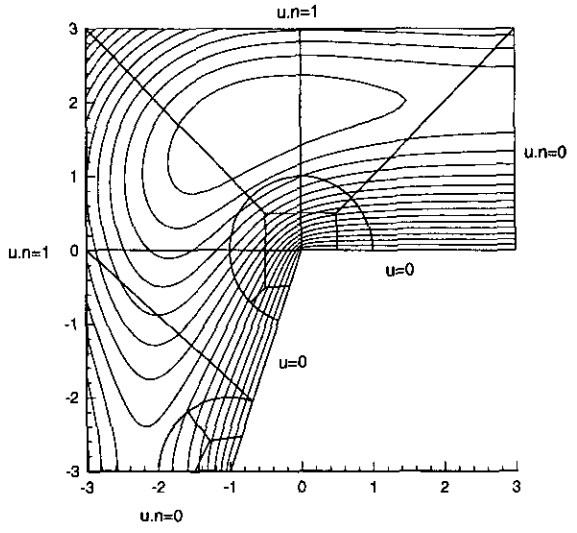

FIG. 10. Domain and boundary conditions for the problem $\nabla^2 u = 1$ of Example 4.2.

domain into two: Ω_1 consists of the six large elements away from the corner; Ω_2 is the nine-element circular sector near the corner. The exact solution is $u = y(y - 3x)/2$, which is analytic in x and y but which has leading order $\rho^{2\alpha} \approx \rho^{2.795}$ as $\rho \to 0$ in the ξ-plane. The expected error decay after mapping in Ω_2 is therefore $O(N^{-5.590})$, and we compute a decay rate of $O(N^{-6.09})$, whereas we obtain exponential convergence if we do not apply any treatment (Fig. 9).

EXAMPLE 4.2. A more typical scenario comes from solving $\nabla^2 u = 1$ on the same geometry as in the above example, but using boundary conditions similar to those used for Laplace's equation of Example 3.1. In this case we decompose the domain into three subdomains since both corners at (0, 0) and (−1, −3), give rise to singular effects (Fig. 10). We let Ω_1 be the background domain as usual, Ω_2 the sector close to the origin, and Ω_3 the sector with vertex at (−1, −3). In this case the exact solution is not known, so errors were calculated using a benchmark solution computed with $N = 27$. Although the mapping is highly beneficial, it is not sufficient to obtain an exponential rate of convergence (Fig. 11). The decay of the coefficients in the asymptotic expansions (11) is only algebraic.

The natural thing to do is to try to separate the component of the solution that is regular in the z-plane from the one that is regular in the ξ-plane. The approach taken by Wigley in finite difference solutions of the Poisson equation was to obtain an estimate of the coefficient of the leading singular terms and to then subtract its contribution out of the boundary values [26]. The solution/subtraction process was iterated until the remaining boundary values were sufficiently smooth to allow an accurate finite difference calculation [27, 28]. Another approach is to supplement the usual polynomial basis with the most singular basis functions. However, the trial functions are no longer orthogonal, and the matrix system to be solved (possibly in a least-squares sense) becomes increasingly ill-conditioned as more singular basis functions are added. Nevertheless, experience shows that using just one or two singular functions is sufficient for dramatic improvements in the convergence.

First consider the case of constant forcing,

$$\nabla^2 u = \mu$$

for some constant μ. The leading singular behaviour at the

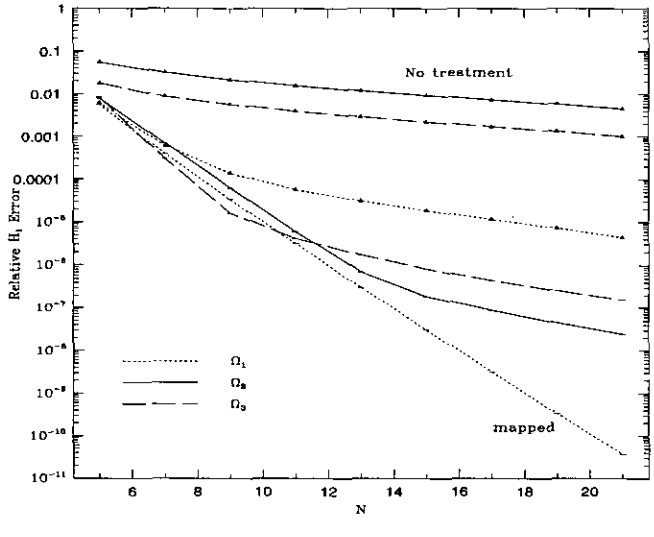

FIG. 11. Relative $\mathcal{H}_1$ errors for the problem $\nabla^2 u = 1$, of Example 4.2, for each of the domains Ω_1, Ω_2, and Ω_3, is the case where (a) no mapping treatment has been applied to any of the domains and (b) mapping has been applied on Ω_2 and Ω_3.

TABLE I

Leading Asymptotic Behaviour for the Singular Solution as $r \to 0$

Angle	Leading behaviour
$0 < \alpha < \frac{1}{2}$	$\underline{r^2}$, then $r^{1/\alpha}$
$\alpha = \frac{1}{2}$	$\underline{r^2 \log r}$, then r^2, then r^4
$\frac{1}{2} < \alpha < \frac{3}{2}$	$r^{1/\alpha}$, then $\underline{r^2}$, then $r^{2/\alpha}$
$\alpha = \frac{3}{2}$	$r^{2/3}$, then $r^{4/3}$, then $\underline{r^2 \log r}$, then r^2
$\frac{3}{2} < \alpha \leq 2$	$r^{1/\alpha}$, then $r^{2/\alpha}$, then $r^{3/\alpha}$.

origin will generally be $u \sim r^{1/\alpha}$, and the error will behave as $\|u - u_N\|_{\mathcal{H}^1(\Omega)} \sim N^{-2/\alpha}$. What we note is that augmenting the basis is much more effective *after* applying conformal mapping. In this case, the leading singular behaviour will be $u \sim r^{2\alpha}$, and the error behaves as $\|u - u_N\|_{\mathcal{H}^1(\Omega)} \sim N^{-4\alpha}$.

For $\nabla^2 u = \mu$, on the prototype domain, the solution has the leading order behaviour listed in Table I, where the contributions due solely to the forcing (when the boundary conditions are homogeneous) are underlined. These results are compatible with those results given in [18]; the important thing to note is how the presence of the forcing complicates the treatment of the singularities. Suppose $\alpha \neq \frac{1}{2}, \frac{3}{2}$. Then $u \in \mathcal{H}^{1/\alpha+1-\varepsilon}$ on the unmapped domain, and the convergence rate is $\|u - u_N\|_1 \sim N^{-2/\alpha-\varepsilon}$. On the mapped domain, $u \in \mathcal{H}^{2\alpha+1-\varepsilon}$ and $\|u - u_N\|_1 \sim N^{-4\alpha-\varepsilon}$. If, in addition, we subtract out the now-singular component, the remaining solution is analytic and we expect exponential convergence. Consequently, the recommendations would be (in order of preference):

$\alpha < 1/\sqrt{2}$: Map and subtract; unmapped; mapped.

$\alpha > 1/\sqrt{2}$: Map and subtract; mapped; unmapped.

$\alpha = \frac{1}{2}$: Unmapped and subtract; mapped and subtract; unmapped; mapped.

$\alpha = \frac{3}{2}$: Map and subtract; mapped; unmapped and subtract; unmapped.

For example, for $\alpha > 1/\sqrt{2}$ with $\alpha \neq \frac{3}{2}$, the appropriate action would be to make the transformation $\xi = z^{1/\alpha}$, subtract the contribution of the leading singular term (proportional to $\rho^{2\alpha}$ as given in Appendix A) from the boundary condition, solve the mapped problem, and return to the physical space $z = \xi^\alpha$, adding back the subtracted function to the solution. The mapping alone increases in power as $\alpha \to 2$, and the advantages of subtraction become weaker, even though the method formally achieves exponential accuracy.

4.1. *Generalization for Variable Forcing*

A general expression can be found for the solution of Poisson's equation as in [24], under mild regularity restrictions on $f(x, y)$. Writing $f = f(r, \theta)$ as

$$f(r, \theta) = \sum_{k=1}^{\infty} f_k(r) \sin\left(\frac{k}{\alpha}\theta\right) = \sum_{k=1}^{\infty}\sum_{l=0}^{\infty} f_{kl} r^l \sin\left(\frac{k}{\alpha}\theta\right),$$

it follows that

$$u(r, \theta) = w(r, \theta) + \sum_{k=1}^{\infty} r^{k/\alpha} \sin\left(\frac{k}{\alpha}\theta\right), \tag{15}$$

where

$$w(r, \theta) = \sum_{k=1}^{\infty}\sum_{l=0}^{\infty} f_{kl}\psi_{kl}(r, \theta)$$

$$\psi_{kl}(r, \theta) = \begin{cases} \dfrac{\alpha^2}{\alpha^2(l+2)^2 - k^2} r^{l+2} \sin\left(\dfrac{k}{\alpha}\theta\right), & k/\alpha \neq l+2, \\ \dfrac{1}{2\alpha(k+1)} r^{k/\alpha} \ln r \sin\left(\dfrac{k}{\alpha}\theta\right), & k/\alpha = l+2. \end{cases}$$

It is readily verified that $\nabla^2 w = f$ and, hence, $\nabla^2 u = f$. Moreover, it is seen that $u(r, \theta) = 0$ on $\theta = 0, \alpha\pi$. However, the expansions (15) are not favored for computational purposes since they are slow to converge when, say, f is analytic in x and y. The eigenfunctions vanish on the wedge walls, while f generally will not. For instance, the expansion for $f = 1$ is

$$f_k(r) = \frac{\alpha}{k}(1 - (-1)^k) = O\left(\frac{1}{k}\right)$$

which is slow; moreover, the convergence is not uniform and one could expect to see the Gibbs phenomenon near the boundaries. Rather than expand the smooth component in terms of the mapped variables, one may try to find explicitly the function w that satisfies $\nabla^2 w = f$ and vanishes on the wedge walls (see Appendix A) and subtract it from the computation procedure. Doing so does not guarantee spectral convergence (due to the nonhomogeneous boundary conditions on Γ_2), but numerical evidence indicates these effects are milder.

It should be remarked that very often, one does not have an explicit expression for the forcing function; rather it is specified through numerical point values. This is the case, for instance, when the equation arises in the numerical solution of the Navier–Stokes problem, where a splitting formulation gives rise to a pressure equation of the form

$$\nabla^2 p = f(x, y),$$

where $f(x, y)$ is related to the velocity field. Assume that $f(x, y)$ is reasonably smooth. In the spectral element approximation, it will have a bivariate polynomial expansion in terms of x and y. The leading coefficients of this expansion are readily calculable, and from these the appropriate subtraction can be determined.

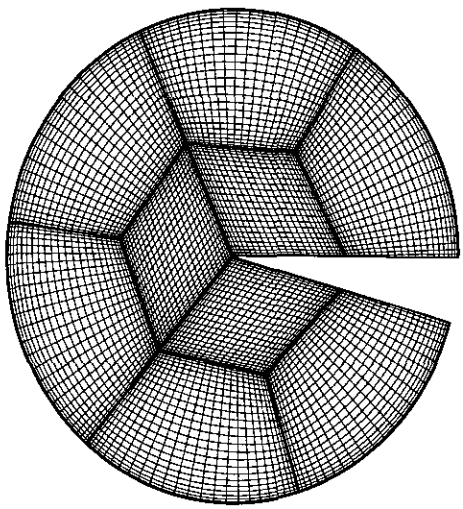

FIG. 12. The spectral element discretization, with $N = 27$, of the geometry for the Helmholtz example 5.1.

5. HELMHOLTZ EQUATION

We shall consider the Helmholtz equation

$$\nabla^2 u - \lambda u = f(x, y), \tag{16}$$

λ a constant, on the domain Ω subject to the usual boundary conditions $u|_{\Gamma_1} = 0$ and $u|_{\Gamma_2} = g(x, y)$. The solution, with arbitrary analytic forcing and boundary conditions, is of the form

$$u(z, \bar{z}) = U(z, \bar{z}, z^{1/\alpha}, \bar{z}^{1/\alpha}, \ln(z), \ln(\bar{z})),$$

where U is a multivariate series, and the terms involving $z^{1/\alpha}$ are the ones that will usually be the source of slow convergence.

There are several potential strategies for increasing the rate of error decay. The conformal mapping described in the two preceding sections is an effective way of improving the convergence rate here as well. The auxiliary mapping $z = \xi^\alpha$ converts the Helmholtz problem (16) to

$$\nabla^2 u - \lambda\alpha^2\rho^{2\alpha-2}u = \alpha^2\rho^{2\alpha-2}f$$

with boundary conditions expressed in terms of the new coordinates. Incorporating this mapping in the linear solver simply requires multiplication by the variable coefficient $\alpha^2\rho^{2\alpha-2}$ when computing the mass matrix and the drive force.

EXAMPLE 5.1. To begin, we illustrate the effectiveness of mapping with the Helmholtz equation

$$\nabla^2 u - u = 1$$

on the circular sector with radius $R = 1$ and $\alpha = \frac{23}{12}$, which defines a very sharp re-entrant corner (Fig. 12). Homogeneous boundary conditions are imposed on all sides. The exact solution is not known in this case, so we use $N = 27$ as our benchmark and estimate the errors for $N = 3, 5, 7, \ldots, 17$. Since the forcing is of the form $\rho^{2\alpha-2}$, by the shift theorem, the best leading order term for $u(\rho, \phi)$ will be $\rho^{2\alpha}$ and the error is expected to decay as $N^{-4\alpha-\varepsilon}$. The results, on the nine-element domain shown in Fig. 12 are in good agreement with theoretical predictions (Table II).

Unlike Laplace's equation, the fundamental solutions for the homogeneous Helmholtz problem do not gain analyticity through the mapping. The general solution of the problem

$$\nabla^2 u - \lambda u = 0 \tag{17}$$
$$u|_{\Gamma_1} = 0, \quad u|_{\Gamma_2} = g(x, y).$$

in the vicinity of the corner has the form

$$u(r, \theta) = \begin{cases} \sum_{k=1}^{\infty} a_k J_{k/\alpha}(\sqrt{-\lambda}r)\sin(k/\alpha\theta), & \lambda < 0, \\ \sum_{k=1}^{\infty} a_k I_{k/\alpha}(\sqrt{\lambda}r)\sin(k/\alpha\theta), & \lambda > 0, \end{cases}$$

when $k/\alpha \neq \mathbb{Z}$. Here J and I represent the Bessel and modified Bessel functions of the first kind, respectively; the functions of the second kind do not appear in the expansion owing to the vanishing boundary conditions. Upon mapping, the solution has the form

$$u(\rho, \phi) = \sum_{k=1}^{\infty} a_k \rho^k \sin(k\theta)\left(\sum_{j=0}^{\infty} c_j \rho^{2j\alpha}\right)$$

with leading singular term of order $\rho^{1+2\alpha}$. Consequently, the estimated convergence rate is

$$\|u - u_N\|_\infty = O(N^{-2-4\alpha-\varepsilon}),$$

which is very fast, although algebraic, for $\alpha > 1$.

Mapping, quite effective alone, is even more so when used in conjunction with other treatments such as supplementary basis functions whose use goes back to 1967 [8]. Supplementary functions of the form $r^{k/\alpha}\sin(k/\alpha\theta)$ have been used in finite-

TABLE II

Error Decay for the Helmholtz problem $\nabla^2 u - u = 1$ on the Circular Sector ($\alpha = \frac{23}{12}$) with Homogeneous Boundary Conditions

Method	Estimated error decay	Experimental error decay
Unmapped	$\|u - u_N\|_\infty \leq cN^{-1.0435}$	$\|u - u_N\|_\infty \approx 0.0501626\ N^{-1.2449}$
Mapped	$\|u - u_N\|_\infty \leq cN^{-7.66667}$	$\|u - u_N\|_\infty \approx 2.31877\ N^{-8.19084}$

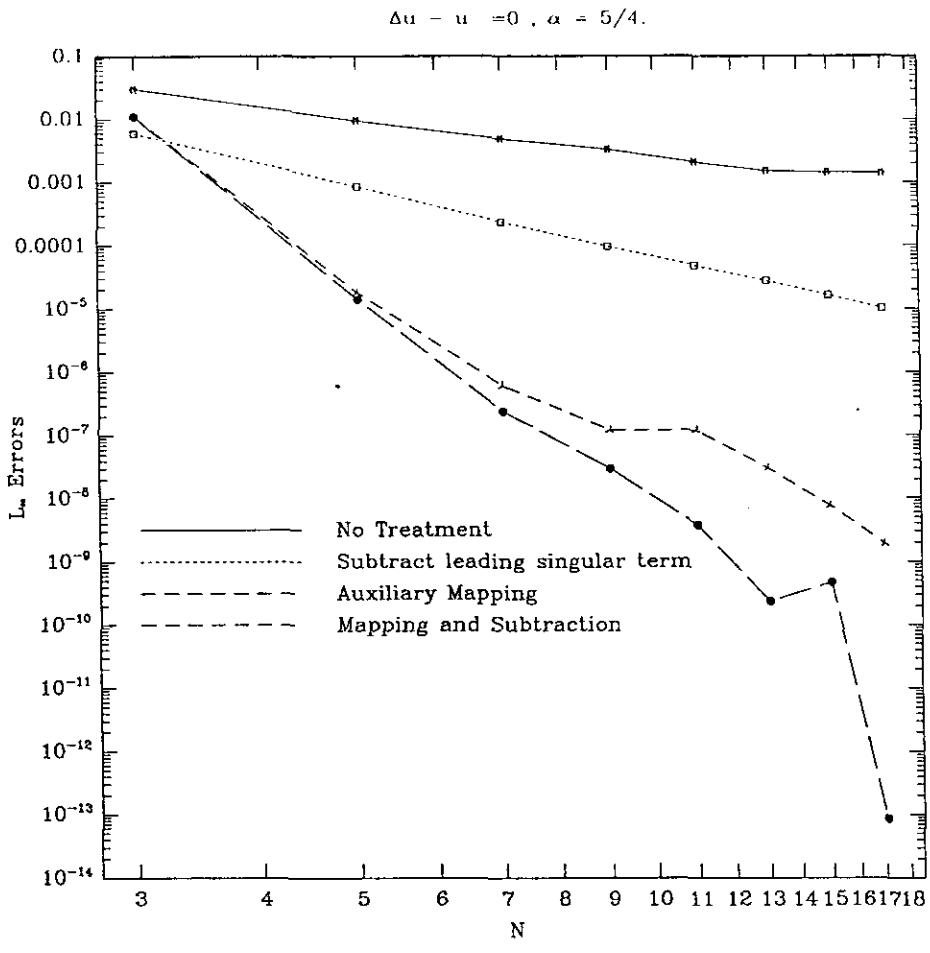

FIG. 13. Relative $\mathcal{H}_1$ errors for $\nabla^2 u - u = 0$ with $\alpha = \frac{5}{4}$, mapped and unmapped treatments with and without subtraction.

element solutions of Laplace's or Poisson's equation [25, 19, 24, 6,] where they extend globally across elemental interfaces with various blending strategies ensuring decay away from the singular corner. Li [15] used a singular basis function expansion, coupled with a domain decomposition for the homogeneous Helmholtz equation. For spectral approximations, supplementary basis functions have been used by Schultz, Lee, and Boyd in solving the biharmonic equation in reference to the driven cavity problem [22], finding that only one or two supplementary functions are needed since the less singular terms can be well approximated by the usual Chebyshev basis.

Let us denote by

$$\{\phi_1(x, y), \phi_2(x, y), \phi_3(x, y), \ldots\}$$

the usual polynomial basis, and by

$$\{\psi_1(x, y), \psi_2(x, y), \psi_3(x, y), \ldots\}$$

the additional singular basis function to be included. Let us work with the homogeneous problem and assume that $\lambda > 0$ (if $\lambda < 0$, the analysis is the same, with the Bessel function J replacing the modified Bessel function I). Then, in the neighborhood of the singularity, the solution has the form

$$u(r, \theta) = \sum_{k=1}^{\infty} a_k I_{k/\alpha}(\sqrt{\lambda} r)\ \sin(k/\alpha\theta)$$

$$= \sum_{k=1}^{\infty} \sum_{l=0}^{\infty} b_{kl} r^{k/\alpha + 2l}\ \sin(k/\alpha\theta),$$

with leading order singular terms

$$r^{1/\alpha}, r^{2/\alpha}\,(\alpha > \tfrac{1}{2}), r^{3/\alpha}\,(\alpha > 1), r^{4/\alpha}\,(\alpha > \tfrac{3}{2}), r^{1/\alpha+2}, \ldots.$$

By including just a few of these, we can significantly improve the convergence rate. In Table III, we list the effects of removing 0, 1, or 2 singular functions, giving the leading singular term of the remainder, and the expected convergence rates.

Now consider supplementing the usual basis in the mapped domain. The local behaviour of the solution is given by

TABLE III

Leading Singular Behaviour and Convergence Rates after Removing the Leading Singular Terms

Number	Basis function	Leading singular term	Convergence rate
0	—	$r^{1/\alpha}$	$N^{-2/\alpha}$
1	$r^{1/\alpha}\sin(1/\alpha\theta)$	$r^{2/\alpha}$	$N^{-4/\alpha}$
	$I_{1/\alpha}(\sqrt{\lambda}r)\sin(1/\alpha\theta)$	$r^{2/\alpha}$	$N^{-4/\alpha}$
2	$\{r^{1/\alpha}\sin(1/\alpha\theta),\ r^{2/\alpha}\sin(2/\alpha\theta)\}$	$r^{3/\alpha}$	$N^{-6/\alpha}$
	$\{I_{1/\alpha}(\sqrt{\lambda}r)\sin(1/\alpha\theta),\ I_{1/\alpha}(\sqrt{\lambda}r)\sin(1/\alpha\theta)\}$	$r^{3/\alpha}$	$N^{-6/\alpha}$

$$u(\rho,\phi)=\sum_{k=1}^{\infty}a_kI_{k/\alpha}(\sqrt{\lambda}\rho^{\alpha})\ \sin k\phi=\sum_{k=1}^{\infty}\sum_{l=0}^{\infty}b_{kl}\rho^{k+2l\alpha}\sin k\phi,$$

so the leading singular terms are

$$\rho^{1+2\alpha},\ \rho^{2+2\alpha}(\alpha>\tfrac{1}{2}),\ \rho^{1+4\alpha},\ \rho^{3+2\alpha}(\alpha>1),\ \ldots.$$

The effects of adding auxiliary functions to the basis are shown in Table IV.

The conclusion is that augmentation is more effective in the mapped domain and that only one or two basis functions need to be included to obtain very fast convergence.

There are two ways of proceeding: by incorporating the singular functions directly in the discrete approximation expansion, or by explicitly removing the most singular terms and then solving for the smoother part. If we follow the first approach and discretize the problem with the augmented basis, we continue with the variational approach generally employed by the spectral element method. The preferability of the variational formulation, as opposed to patching, is clear for these problems, since explicit enforcement of C^1 matching is absolutely inappropriate. The variational statement for the Helmholtz problem is

TABLE IV

Leading Singular Behaviour and Convergence Rates after Removing the Leading Singular Terms after Mapping

Number	Basis function	Leading singular term	Convergence rate
0	—	$\rho^{1+2\alpha}$	$N^{-2-4\alpha}$
1	$\rho^{1+2\alpha}\sin\phi$	$\rho^{2+2\alpha}$	$N^{-4-4\alpha}$
	$I_{1/\alpha}(\sqrt{\lambda}\rho^{\alpha})\sin\phi$	$\rho^{2+2\alpha}$	$N^{-4-4\alpha}$
2	$\{\rho^{1+2\alpha}\sin\phi,\ r^{2+2\alpha}\sin 2\phi\}$	$\rho^{1+4\alpha}$	$N^{-2-8\alpha}$
	$\{I_{1/\alpha}(\sqrt{\lambda}\rho^{\alpha})\sin\phi,\ I_{2/\alpha}(\sqrt{\lambda}\rho^{\alpha})\sin 2\phi\}$	$\rho^{3+2\alpha}$	$N^{-6-4\alpha}$

$$\int\int_{\Omega}\nabla u\cdot\nabla v\,d\xi_1d\xi_2+\lambda\int\int_{\Omega}\rho^{2\alpha-2}uv\,d\xi_1d\xi_2=-\int\int_{\Omega}\rho^{2\alpha-2}fv\,d\xi_1d\xi_2.$$

Let us write

$$u=\sum_{j=1}^{N_1}\phi_j(\xi_1,\xi_2)+\sum_{n=1}^{N_2}\psi_n(\xi_1,\xi_2),$$

where ϕ_j .are the usual Gauss–Legendre–Lobatto polynomial basis (after mapping to the standard square) and where ψ_n are the (fewer) singular basis functions. Recall that for Gauss–Lobatto–Legendre integration of the function $F(x)\in C^{2n-2}[-1,1]$ has the error term $O(F^{2n-2}(x^*))$, where $-1\le x^*\le 1$, using an integration rule of degree greater than n. Open formulas are usually more effective when the singular point lies at the domain endpoint, although the Gauss–Radau formula, for instance, still has the same formal order of convergence. It is advised to form the inner products analytically when possible [24], since these are not smooth. The θ-dependence and inner products of the form (ϕ_i,ψ_j) can possibly be computed by high order interpolation. Second, there is the question of inverting the stiffness matrix. If many singular functions are used, the matrices become ill-conditioned as the complete basis $\{\phi_1,\phi_2,\ldots,\phi_{N_1},\psi_1,\psi_2,\ldots,\psi_{N_2}\}$ is nearly linearly dependent.

An alternative method is to explicitly subtract out the leading singularity, as done by Schultz, Lee, and Boyd [22]. Whereas, for their problem the coefficients of the leading singular term were exactly known, in our case they must be estimated numerically. We have the asymptotic behaviour

$$u=\sqrt{2/\pi}\sum_{k=1}^{\infty}a_kI_{k/\alpha}(\sqrt{\lambda}\rho^{\alpha})\ \sin k\phi.$$

On the semi-circle, the coefficients are determined by the boundary condition $u|_{\Gamma_2}=g(\phi)$,

$$a_kI_{k/\alpha}(\sqrt{\lambda}R^{\alpha})=\sqrt{2/\pi}\int_0^{\pi}g(\phi)\ \sin k\phi d\phi,$$

and for the leading singular term

$$a_1I_{1/\alpha}(\sqrt{\lambda}R^{\alpha})=\sqrt{2/\pi}\int_0^{\pi}g(\phi)\ \sin\phi d\phi.$$

Let $u=u_s+\psi_1$, where u_s has leading order term $\rho^{2+2\alpha}$ and

$$\psi_1(\rho,\phi)=\sqrt{2/\pi}a_1I_{1/\alpha}(\sqrt{\lambda}\rho^{\alpha})\ \sin\phi=\frac{2}{\pi}\left[\frac{I_{1/\alpha}(\sqrt{\lambda}\rho^{\alpha})}{I_{1/\alpha}(\sqrt{\lambda}R^{\alpha})}\right]\left[\int_0^{\pi}g(\phi)\ \sin\phi d\phi\right]\sin\phi$$

TABLE V

Error Decay for the Helmholtz Problem $\nabla^2 u - u = 0$ on the Circular Sector with $\alpha = \frac{5}{4}$ with Boundary Conditions $u|_{\Gamma_2} = \theta^2 \sin(\theta - \frac{5}{4}\pi)$

Method	Estimated error decay	Experimental error decay
No treatment	$\|u - u_N\|_\infty \le cN^{-1.6}$	$\|u - u_N\|_\infty \approx 0.19544\ N^{-1.84602}$
Subtract out leading term	$\|u - u_N\|_\infty \le cN^{-3.2}$	$\|u - u_N\|_\infty \approx 0.30958\ N^{-3.6526}$
Mapping	$\|u - u_N\|_\infty \le cN^{-7}$	$\|u - u_N\|_\infty \approx 24.5782\ N^{-8.26055}$
Mapping and subtraction	$\|u - u_N\|_\infty \le cN^{-9}$	$\|u - u_N\|_\infty \approx 13970.8\ N^{-12.5484}$

is the most singular term. Instead of solving the given problem, we solve

$$\nabla^2 u_s - \lambda u_s = 0,$$

$$u_s|_{\Gamma_1} = 0, \quad u_s|_{\Gamma_2} = g - \psi_1|_{\Gamma_2} = g - \frac{2}{\pi}\int_0^\pi g(\phi)\ \sin\phi d\phi,$$

and add $a_1\psi_1$ to the numerical result to obtain the desired solution u.

EXAMPLE 5.2. (Table V). We solve the homogeneous problem

$$\nabla^2 u - u = 0$$

on the wedge of radius 1 and angle $\frac{5}{4}\pi$, subject to the boundary conditions $u|_{\Gamma_1} = 0$, and

$$u|_{\Gamma_2} = \theta^2 \sin(\theta - \tfrac{5}{4}\pi) = \tfrac{25}{16}\phi^2 \sin(\tfrac{5}{4}(\phi - \pi)).$$

Then

$$a_1 I_{1/\alpha}(1) = \sqrt{2/\pi}\,\tfrac{25}{56}\int_0^\pi \theta^2 \sin(\tfrac{5}{4}(\phi - \pi))\ \sin(\phi)\, d\phi \approx$$

$$-4.42865033179881902.$$

We therefore solve the problem

$$\nabla^2 u_s - u_s = 0$$

$$u_s|_{\Gamma_1} = 0,$$

$$u_s|_{\Gamma_2} = \theta^2 \sin(\theta - 5\pi/4)$$

$$+ 4.42865033179881902 \sin(4/5\,\theta).$$

We do observe an improvement in the convergence rate using the subtraction method. The point is that the error decays so quickly through the mapping alone, that the benefit is questionable. The errors in Table V were computed using points lying within a radius 0.4 of the origin in the relevant domain and are based on all cases $N = 3, 5, \ldots, 17$, compared with an $N = 27$ benchmark solution. The maximum point-wise error between the mapped solutions, $N = 27$, with and without subtraction was 2.5427×10^{-10}, at $\xi_1 = \xi_2 = \sqrt{2}$. The results are much less reassuring in the unmapped case, where the maximum error is 5.0152×10^{-4} at the point $x = -9.9871 \times 10^{-4}$, $y = 2.4111 \times 10^{-3}$. The error occurs near the singular corner without the mapping and on the edge of the domain with it.

We comment that the mapping alone is highly effective in this case; its value is slightly weaker as α is decreased.

6. CONCLUSIONS

In this paper we have presented some methods for obtaining high-order solutions of elliptic boundary value problems in domains containing singular boundary data. These algorithms are developed in the context of spectral element methods which, for smooth solutions, have convergence rates that are better than algebraic, but which lose this advantage in the presence of singularities. The main idea here is to weaken the singularity through auxiliary mapping and *then* to augment the spectral element basis with singular basis functions.

This basic idea is easily generalized. If one has a treatment for a singularity of the type considered here, it may be more effectively applied in the mapped coordinate system where the singularity is less strong. The use of graded meshes, for example, is one such treatment where the degree of gradation (and hence the cost) is reduced by operating in the semicircular ξ domain [7]. The same is true when the graded meshes are combined with polynomials of varying degree, where the total number of degrees of freedom required decreases with the strength of the singularity [1]. Moreover, this approach is not restricted to the equations shown here, but is applicable whenever one knows the leading term of the asymptotic expansion of the singular solution.

APPENDIX A

The duality between Laplace's equation with smooth boundary conditions on Γ_2 and Poisson's equation,

$$\begin{aligned} &\nabla^2 u = f(x, y), \\ &u|_{\Gamma_1} = 0, \quad u|_{\Gamma_2} = g(x, y), \end{aligned} \tag{18}$$

where f is smooth, can be seen by writing the solution of (18) as $u = v + w$, where v is a singular solution of Laplace's equation while w is a smooth solution of Poisson's equation.

We begin with the simplest case, when the forcing is some constant value μ,

$$\nabla^2 u = \mu$$

and the solution vanishes along Γ_1. Following [18], we have that, for $\alpha \neq 1/2, 3/2$,

$$u(r,\theta)=\frac{r^2\mu}{4}\left(1-\frac{\cos(2\theta-\alpha\pi)}{\cos\alpha\pi}\right)+\sum_{k=1}^{\infty}a_k r^{k/\alpha}\sin\left(\frac{k}{\alpha}\theta\right), \quad (19)$$

so here $w(r, \theta)$, the first term, is analytic, while v, the singular sum, is in $\mathcal{H}^{1/\alpha+1-\varepsilon}(\Omega)$ for any $\varepsilon > 0$. When $\alpha = \frac{1}{2}$ or $\alpha = \frac{3}{2}$, the "smooth" solution w actually contains logarithmic terms, since

$$u(r,\theta)=\frac{\mu r^2}{4\alpha\pi}(\alpha\pi+2\ln r\sin(2\theta)+(2\theta-\alpha\pi)\cos(2\theta)) + \sum_{k=1}^{\infty}a_k r^{k/\alpha}\sin\left(\frac{k}{\alpha}\theta\right), \quad (20)$$

respectively. The coefficients a_k in (19) and (20) are determined by the global boundary conditions.

In general, for $f(x, y) \in \mathcal{H}^m(\Omega)$, u can be decomposed as $u = w + v$, where $w(x, y) \in H^{m+2}(\Omega)$ and $v(x, y) = \sum_k c_k\psi_k(x, y)$ with ψ_k denoting the fundamental solutions (9) [10]. Now if w is a solution of Poisson's equation that vanishes on the wedge walls, it follows that v satisfies Laplace's equation, vanishes on the wedge walls, and

$$v|_{\Gamma_2} = g(\theta) - w|_{\Gamma_2}.$$

Using the auxiliary mapping technique, v can therefore be computed with spectral accuracy if $v|_{\Gamma_2}$ is such that the solution is smooth in the mapped variables.

To find w, let $\partial/\partial\tau_i$ denote differentiation in the direction tangential to the wall

$$\frac{\partial^k}{\partial\tau_1^k}=\left.\frac{\partial^k}{\partial r^k}\right|_{\theta=0}, \quad \frac{\partial^k}{\partial\tau_2^k}=\left.\frac{\partial^k}{\partial r^k}\right|_{\theta=\alpha\pi}.$$

Then $w \in \mathcal{H}^{m+2}(\Omega)$ when w is such that

$$\left[\frac{\partial^k}{\partial\tau_i^k}\nabla^2 w=\frac{\partial^k}{\partial\tau_i^k}f\right]_{\Gamma} \quad (21)$$

for $k = 0 \ldots m$. A direct way of satisfying these compatibility conditions is to find w such that $\nabla^2 w = f$ in Ω and $w = 0$ on the walls. For certain forcings, this is easy. For instance, when $p \neq 0$,

$$f = r^{p-2} \leftrightarrow w(r,\theta)$$

$$=\frac{1}{p^2}r^p\left(1-\frac{\cos(p\theta-p/2\alpha\pi)}{\cos(p/2\alpha\pi)}\right)$$

$$f = r^{p-2}\sin(2p\theta-\alpha\pi) \leftrightarrow w(r,\theta)$$

$$=\frac{2}{3p^2}r^p\sin(p\theta-p/2\alpha\pi)(\cos(p/2\alpha\pi)-\cos(p\phi-p/2\alpha\pi))).$$

To generalize, let us assume that the forcing is analytic in x and y, with expansion

$$f(x,y)=\sum_{m=0}^{\infty}\sum_{n=0}^{\infty}d_{nm}x^n y^m. \quad (22)$$

If we make the ansatz

$$w(x,y)=\sum_{m=0}^{\infty}\sum_{n=0}^{\infty}a_{mn}y^m(y-cx)^n, \quad (23)$$

then w is analytic, and $w|_{\Gamma_1} = 0$ if we choose $c = \tan(\alpha\pi)$. We shall assume that $c \neq 0$, that is, $\alpha \neq 0, 1$. These cases correspond to the uninteresting situation when there is no corner at all, and hence no singularity. Then we must find $\{a_{mn}\}$ so that $\nabla^2 w = f$. Two useful examples are

$$\left.\begin{aligned} a_{12} &= -\frac{3}{2c(3-c^2)}\\ a_{21} &= \frac{3+c^2}{2c(3-c^2)}\\ a_{mn} &= 0 \quad \text{otherwise}\end{aligned}\right\} \Rightarrow f(x,y)=x, \quad (24)$$

$$\left.\begin{aligned} a_{12} &= -\frac{1}{2(3-c^2)}\\ a_{21} &= \frac{1}{(3-c^2)}\\ a_{mn} &= 0 \quad \text{otherwise}\end{aligned}\right\} \Rightarrow f(x,y)=y. \quad (25)$$

Under what conditions can we find an expansion of the form (23) given a forcing of the form (22)? For convenience, let us introduce new independent variables $(x, y) \leftrightarrow (\xi, \eta)$ through the invertible transformation $\eta = y$ and $\xi = y - cx$. Then the Laplacian of

$$w(\xi,\eta)=\sum_{m=1}^{\infty}\sum_{n=1}^{\infty}a_{mn}\eta^m\xi^n$$

can be written as $\nabla^2 w = \sum_{m=0}^{\infty}\sum_{n=0}^{\infty}[(m+1)(m+2)a_{m+2,n} + 2(m+1)(n+1)a_{m+1,n+1} + (c^2+1)(n+1)(n+2)a_{m,n+2}]\eta^m\xi^n$ if we define $a_{m0} = a_{0n} = 0\ \forall m, n \in \mathbf{Z}$. Now $f(x, y)$ can be written as

$$f(\xi,\eta)=\sum_{m=0}^{\infty}\sum_{n=0}^{\infty}b_{mn}\eta^m\xi^n,$$

and equating coefficients of like powers in $\nabla^2 w$ and f requires satisfying the linear equations

$$(m+1)(m+2)a_{m+2,n} + 2(m+1)(n+1)a_{m+1,n+1} + (c^2+1)(n+1)(n+2)a_{m,n+2} = b_{mn} \quad (26)$$

$\forall m, n \geq 0$.

To determine whether the system (26) is nonsingular, we impose an ordering according to the degree of the monomial $\xi^m \eta^n$, i.e., according to the sum of the subscripts $s = m + n$. In this way our system decouples into independent blocks of dimension $(s+1) \times (s+1)$, for $s = 0, 1, \ldots$. Consider a fixed s and then impose a subordering with $m = 0, 1, \ldots, s$. The linear system to be solved is $M\mathbf{a} = \mathbf{b}$, where M is the $(s+1) \times (s+1)$ tridiagonal matrix defined by

$$M_{ml} = \begin{cases} (c^2+1)(s-m+1)(s-m+2), & l = m-1, \\ 2(m+1)(s-m+1), & l = m, \\ (m+1)(m+2), & l = m+1, \end{cases}$$

with $0 \leq m, l \leq s$. This block corresponds to matching the degree s terms in the Laplacian and in the forcing; the relevant term in the solution ansatz are of degree $s+2$.

To compute the determinant of the matrix M, we let M_j be its upper left $(j+1) \times (j+1)$ block for $j = 0, \ldots, s$. The corresponding determinant D_j satisfies

$$D_j = 2(j+1)(s-j+1)D_{j-1} - (c^2+1)(s-j+1)(s-j+2)j(j+1)D_{j-2}.$$

Letting $\beta_j = D_j(s-j)!/(j+1)!$, we find that β_j satisfies the recurrence relation

$$\beta_j = 2\beta_{j-1} - (c^2+1)\beta_{j-2}.$$

Using the appropriate starting values β_0 and β_1, we have then that

$$\beta_j = \frac{(c^2+1)^{j/2}(s+1)!}{c}(2c\cos(j\tan^{-1}c) + (1-c^2)\sin(j\tan^{-1}c)),$$

and the matrix $M = M_s$ is singular if $D_s = 0$, or, equivalently, if $\beta_s = 0$. Recalling that $c = \tan(\alpha\pi)$, this is the case if

$$2\tan(\alpha\pi) = (\tan^2(\alpha\pi) - 1)\tan(s\alpha\pi). \quad (27)$$

Equation (27) cannot be satisfied if $\tan(\alpha\pi) = \pm 1$, so we can divide through by $(\tan^2(\alpha\pi) - 1)$ and thereby obtain

$$-\tan(2\alpha\pi) = \tan(s\alpha\pi) \quad (28)$$

as the condition for singularity of the matrix. Equation (28) is satisfied in $\alpha = k/(s+2)$ for $k \in \mathbf{Z}$, the case physically corresponding to the alignment of ξ^s with the η axis. These results are compatible with those of [10] and are due to the incompleteness of the regular basis. The logarithmic terms are missing.

ACKNOWLEDGMENTS

We gratefully acknowledge the software and assistance of Ron Henderson, Catherine Crawford, and David Newman. This work was supported by DOE Grant DE-FG02-95ER25239, AFOSR Grant F49620-94-1-0313, and NSF Grant ECS-9023362.

REFERENCES

1. I. Babuska and M. Dorr, *Numer. Math.* **37,** 257 (1981).
2. I. Babuska and H.-S. Oh, *Numer. Methods Partial Differential Equations* **6,** 371 (1990).
3. I. Babuska and M. Suri, *SIAM J. Numer. Anal.* **24,** 750 (1987).
4. W. Cai, D. Gottlieb, and C. Shu, *Math. Comput.* **52**(196), 389 (1989).
5. W. Cai, H. C. Lee, and H.-S. Oh, *J. Comput. Phys.* **108,** 314 (1993).
6. G. F. Carey and J. T. Oden, *Finite Elements: A Second Course,* The Texas Finite Element Series (Prentice-Hall, Englewood Cliffs, NJ, 1983).
7. R. Doucette, *SIAM J. Numer. Anal.* **30**(3), 717 (1993).
8. L. Fox, P. Henrici, and C. Moler, *SIAM J. Numer. Anal.* **4**(1), 89 (1967).
9. D. Funaro, A. Quarteroni, and P. Zanolli, Technical Report 530, Instituto di Analisi Numerica del Consiglio Nazionale delle Ricerche, 1985 (unpublished).
10. P. Grisvard, *Elliptic Problems in Nonsmooth Domains* (Pitman, Boston, 1985).
11. B. Guo and I. Babuska, *Comput. Mech.* **1,** 203 (1986).
12. R. Henderson and G. E. Karniadakis, *J. Sci. Comput.* **6**(2), 79 (1991).
13. G. E. Karniadakis, M. Israeli, and S. A. Orszag, *J. Comput. Phys.* **97**(2), 414 (1991).
14. N. Kikuchi and J. T. Oden, *Contact Problems in Elasticity: A Study of Variational Inequalities and Finite Element Methodology,* SIAM Series in Applied Mathematics (SIAM, Philadelphia, 1988).
15. Z.-C. Li, *J. Comput. Phys.* **89,** 414 (1990).
16. Y. Maday and A. T. Patera, "Spectral Element Methods for the Incompressible Navier–Stokes Equations, in *State-of-the-Art Surveys on Computational Mathematics, Philadelphia, 1989,* edited by A. K. Noor and J. T. Oden, p. 71.
17. J. C. Mason, *SIAM J. Appl. Math.* **15**(1), 172 (1967).
18. H. K. Moffat and B. R. Duffy, *J. Fluid Mech* **96**(2), 299 (1980).
19. L. G. Olson, G. C. Georgiou, and W. W. Schultz, *J. Comput. Phys.* **96,** 391 (1991).
20. A. T. Patera, *J. Comput. Phys.* **54,** 468 (1984).
21. J. K. Reid and J. E. Walsh, *J. Soc. Indus. Appl. Math.* **13,** 837 (1965).
22. W. W. Schultz, N. Y. Lee, and J. P. Boyd, *J. Sci. Comput.* **4,** 1 (1989).
23. D. Sidilkover and G. E. Karniadakis, *J. Comput. Phys.* **107**(1), 10 (1993).
24. G. Strang and G. J. Fix, *An Analysis of the Finite Element Method* (Prentice-Hall, Englewood Cliffs, NJ, 1973).
25. R. Wait and A. R. Mitchell, *J. Comput. Phys.* **8,** 45 (1971).
26. N. M. Wigley, *Math. Comput.* **23,** 395 (1969).
27. N. M. Wigley, *SIAM J. Numer. Anal.* **24**(2), 350 (1987).
28. N. M. Wigley, *J. Comput. Phys.* **78,** 369 (1988).